Optimal propulsion of an undulating slender body with anisotropic friction

Baptiste Darbois Texier, Alejandro Ibarra, Francisco Melo

Soft Matter

Accepted Manuscript

This article can be cited before page numbers have been issued, to do this please use: B. Darbois Texier, A. Ibarra and F. Melo, *Soft Matter*, 2017, DOI: 10.1039/C7SM01545C.

ROYAL SOCIETY OF CHEMISTRY

rsc.li/soft-matter-journal

View Article Online
DOI: 10.1039/C7SM01545C
ROYAL SOCIETY OF CHEMISTRY

Journal Name

ARTICLE TYPE

Cite this: DOI: 10.1039/xxxxxxxxxx

Optimal propulsion of an undulating slender body with anisotropic friction

Baptiste Darbois Texier,[a] Alejandro Ibarra,[a] and Francisco Melo[a]

Received Date
Accepted Date

DOI: 10.1039/xxxxxxxxxx

www.rsc.org/journalname

This study investigates theoretically and numerically the propulsive sliding of a slender body. The body sustains a transverse and propagative wave along its main axis, and undergoes anisotropic friction caused by its surface texture sliding on the floor. A model accounting for the anisotropy of frictional forces acting on the body is implemented. This describes the propulsive force and gives the optimal undulating parameters for efficient forward propulsion. The optimal wave characteristics are effectively compared to the undulating motion of a slithering snakes, as well as with the motion of sandfish lizards swimming through the sand. Furthermore, numerical simulations have indicated the existence of certain specialized segments along the body that are highly efficient for propulsion, explaining why snakes lift parts of their body while slithering. Finally, the inefficiency of slithering as a form of locomotion to ascend a slope is discussed.

1 Introduction

Locomotion is an essential factor in the survival of most living organisms, facilitating feeding, reproduction, and escape from predators. Depending on their capacity and environment animals use different modes of locomotion, most commonly walking, running, jumping, swimming and flying[1–5]. However, in the terrestrial animal kingdom some species are limbless and thus require alternative methods of locomotion[6]. This is the case for slugs and snails which move by means of a pedal locomotory wave, involving the rippling the underside of their body on a thin layer of mucus[7]. Similarly, earthworms move via retrograde waves, alternatively swelling and contracting throughout the length of their body[8].

Due to the versatile nature of snakes body, they are able to adapt their gait according to their situation and terrain[9]. In walled environments a concertina locomotion is observed, where the snake alternately braces sections of its body over the surrounding substrate[10]. Sidewinding occurs on sand or loose soil, where the snake alternates between projecting its front section in the direction of motion and following with the back part in a transverse motion[11,12]. For silent movement, snakes prefer a rectilinear locomotion, where large scales on the underside of the body facilitate propulsion through pushing backwards and downards[13–15]. Finally, over flat surfaces, slithering is achieved through a transversal undulation along the entire body. These four modes of locomotion are also employed by legless lizards[16].

During the last decade there has been considerable theoretical and experimental efforts to understand the physical mechanisms underlying each mode of locomotion. Hu *et al.* identified that the primary propulsive force in slithering is the anisotropy friction force of snake skin against the substrate[17]. The topic of propulsion through optimal lateral undulating motion with an anisotropic friction force has been previously addressed through various approaches. Jing *et al.* studied the optimal motion of both a two-link and a three-link body[18]. For a two-link body, it is observed that with a sufficiently high transverse friction coefficient, the internal angle amplitude to maximize propulsion efficiency is about $\pi/2$. The limits upon bodies with an infinite number of links were addressed by Alben, who used a Chebyshev polynomial decomposition and a numerical optimizing algorithm in order to find the optimal undulating motion of a body subjected to anisotropic friction[19]. It has been found that for intermediate transverse friction coefficients the optimal undulating motion is a backwards traveling wave of sufficiently large amplitude and single wavelength. Furthermore, Guo and Mahadevan introduced internal elasticity and viscosity in order to mimic the effect of muscles in the mechanics of wave propulsion[20].

The problem of an undulating filament subjected to anisotropic forces is also encountered in viscous fluids in the context of microorganism locomotion[21]. Indeed, the flow around a slender body moving at a low Reynolds number induces a larger viscous force for perpendicular motion than for a tangential one[22]. This problem was initially addressed by Gray and Hancock[23] to describe the propulsion of sea urchin spermatozoa, and other studies followed, such as an analysis of the flagellum propulsion or the tridimensional trajectories of sperm cells[24]. However, viscous stress in fluids differs from solid friction since it depends on

[a] *SMAT-C, Departamento de Física de la Universidad de Santiago de Chile, Avenida Ecuador 3493, 9170124 Estación Central, Santiago, Chile; E-mail: bdarbois@usach.cl*

View Article Online
DOI: 10.1039/C7SM01545C

the object velocity and involves the presence of fluid motion at relatively large distance. Thus, the Resistive force theory that neglectes long-range interactions has been proved to poorly describe the propulsion at low Reynolds number. Others methods have been proposed to solve this problem such as the Slender-body theories of Lighthill and Johnson[25] and the regularized Stokeslet method[26].

From a different perspective, investigation into modes of snake locomotion has inspired the development of various snake robots, capable of proceeding through complex environments[27]. However, the optimal motion of an undulating body experiencing anisotropic friction still lacks of simple physical understanding. The present study assumes that a slender body has appropriate internal mechanisms to sustain an undulatory motion, *i.e.* a flexural traveling wave. The aim of this work is to identify the optimal parameters and strategies for efficient propulsion, via the coupling of anisotropic frictional forces with the flexural traveling wave. The model used in this study partially follows the guidelines defined by Hu *et al.*[17], but accounts for anisotropic friction differently through dissipation energy arguments. First, a theoretical model is developed based on anisotropic friction forces in Section 2 and the predictions of the model are considered qualitatively, regarding an optimal configuration for forwards propulsion. Subsequently, the model is solved numerically in Section 3 and the best undulating wave characteristics in terms of speed and energy consumption are determined. In addition, numerical results for snake and sandfish motion are compared with the one reported in the literature. Finally, the numerical simulation is extended in order to include non-uniform mass repartition along the snake's body and inclined substrates.

2 Model

2.1 Kinematics

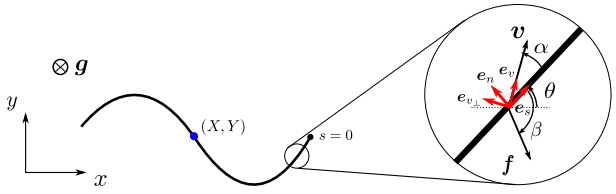

Fig. 1 Notation used to describe the problem of an undulating slender body subjected to anisotropic friction forces.

A snake is modeled by a one-dimensional and inextensible slender body of length L and uniform mass per unit length ρ. The body shape is described by the curvilinear coordinates (s,θ), where s is the curve arc length measured from the head, and θ the local angle of the body respectively to the x-direction as sketched in Fig. 1. The gravity acceleration $\boldsymbol{g}$ applies along the z-direction, which is normal to the plane of motion of the snake. The time evolution of the body shape within the frame of its center of mass is considered to be a flexural traveling wave following $\partial\theta/\partial s(s,t) = \theta_m k\cos(\omega t + ks)$ with θ_m the angular amplitude, k the wavelength and $\omega = 2\pi f$ the pulsation. This expression represents the motion used by Pueblan milk snakes while slithering[17]. In addition to its undulation, the body undergoes an overall motion of its center of mass within the frame of the laboratory, which is characterized by a velocity $\boldsymbol{V} = (\dot{X},\dot{Y})$. Finally, each body segment has a local velocity $\boldsymbol{v}$, which is a composition of the center of mass velocity and the undulating velocity. In the $x,y-$base, the tangential and normal directions of the body are given by the unit vectors $\boldsymbol{e}_s = (\cos\theta,\sin\theta)$ and $\boldsymbol{e}_n = (-\sin\theta,\cos\theta)$ and the tangential and normal directions of the velocity are given by the unit vectors $\boldsymbol{e}_v = (\cos(\theta+\alpha),\sin(\theta+\alpha))$ and $\boldsymbol{e}_{v_\perp} = (-\sin(\theta+\alpha),\cos(\theta+\alpha))$.

2.2 Anisotropic friction force

It is assumed that all segments of the body slide against a substrate and experience solid friction. The friction is considered to be anisotropic and is characterized by a friction coefficient $\mu(\alpha)$, which depends on the angle α made by the local velocity and the direction tangent to the body. Hu *et al.* considered a friction force expression that is the weighted average of the independent friction responses to forwards, backwards and transverse motions[17]:

$$\boldsymbol{f} = -\rho\, g\, [\mu_n(\boldsymbol{e}_v\cdot\boldsymbol{e}_n)\boldsymbol{e}_n + [\mu_s H(\boldsymbol{e}_v\cdot\boldsymbol{e}_s) + \mu_b(1-H(\boldsymbol{e}_v\cdot\boldsymbol{e}_s))]\cdot(\boldsymbol{e}_v\cdot\boldsymbol{e}_s)\boldsymbol{e}_s]\,. \tag{1}$$

where μ_s, μ_b ans μ_n correspond to the forwards, backwards and normal friction coefficients respectively and H is the Heaviside step function used to distinguish between the forwards and backwards directions. This approach is understood to be a result of the generalization of Coulomb's law. However, energetic considerations lead to a different expression of anisotropic frictional forces[28]. Indeed, the work per unit length δW of the force $\boldsymbol{f}$ associated with the a displacement $dl\,\boldsymbol{e}_v$ of a body segment is $\delta W = \boldsymbol{f}\cdot\boldsymbol{e}_v\,dl$. Considering that such a work is dissipated by friction, $\boldsymbol{f}\cdot\boldsymbol{e}_v = -\mu(\alpha)\rho g$ is obtained, which indicates that the projection of the frictional force along the velocity is simply the frictional coefficient of the corresponding direction times the normal force. As demonstrated by Chateau and Géminard[28], through the progressive increase of the norm f of the force, an additional condition providing the minimal frictional force able to produce body motion is obtained from a tangent condition. This condition determines the component of the force perpendicular to the body speed and reads, $\boldsymbol{f}\cdot\boldsymbol{e}_{v_\perp} = -\mu'(\alpha)\rho g$. Finally, the full expression of the friction force per unit length is,

$$\boldsymbol{f} = -\rho\, g\, \left[\mu(\alpha)\,\boldsymbol{e}_v + \mu'(\alpha)\,\boldsymbol{e}_{v_\perp}\right]. \tag{2}$$

Recently, Chateau and Géminard have successfully used Eq. (2) in order to predict the path of a moving disk subjected to anisotropic friction force according to the texture of a substrate[28]. Furthermore, Tapia *et al.* verified the validity of Eq. (2) by measuring the tangential and normal friction force experienced by a slider on a textured surface[29]. Because, these experiments sustain the validity of Eq. (2) compared to Eq. (1), in the following, the friction force provided by Eq. (2) is considered. Independently from the force expression, Hu and colleagues measured the anisotropic friction coefficient of Pueblan milk snakes to be $\mu(\alpha) = \mu_s\cos^2\alpha + \mu_n\sin^2\alpha$, with μ_s and μ_n the forwards and transverse friction coefficients, respectively[17]. This expression of the friction anisotropy has been then used in further studies con-

View Article Online
DOI: 10.1039/C7SM01545C

cerning slithering locomotion[18,19]. Following the experimental determination of $\mu(\alpha)$, it is inferred from Eq. (2) that $\boldsymbol{f}\cdot\boldsymbol{e}_v = -\rho g(\mu_s\cos^2\alpha + \mu_n\sin^2\alpha)$ and $\boldsymbol{f}\cdot\boldsymbol{e}_{v_\perp} = -2\rho g(\mu_n-\mu_s)\cos\alpha\sin\alpha$. It is worth noting that the latter differs by a factor two from the frictional force, perpendicular to the segment speed, predicted by the Eq. (1) proposed by Hu *et al.*[17]. Finally, the angle β made by force and the body tangent (*cf.* Fig. 1), relates to α through the implicit expression,

$$\tan(\beta-\alpha) = \frac{2(\mu_n-\mu_s)\cos\alpha\sin\alpha}{\mu_s\cos^2\alpha+\mu_n\sin^2\alpha}. \tag{3}$$

The speed of each body segment is orientated forwards, and it is not necessary to introduce a backwards friction coefficient, as noted by Hu and Shelley[30].

2.3 Theoretical analysis

Prior to solving numerically the dynamics of a slender body subjected to anisotropic frictional forces, it is useful to first establish qualitatively how anisotropy couples to the propagative wave and results in the forward propulsion force of the body. A single segment of the body is considered with an orientation of θ with respect to the horizontal, as illustrated in the inset of Fig. 1. Assuming that the body is motionless when the propagating wave starts, the segment has a initial velocity which is purely vertical, *i.e.* $\theta+\alpha = \pm\pi/2$. In this instance, the projection of the force experienced by the segment in the x-direction is $\boldsymbol{f}\cdot\boldsymbol{e}_x = 2\rho g(\mu_n-\mu_s)\cos\theta\sin\theta$, which indicates that a greater difference between the friction coefficients leads to a larger initial acceleration of the body segment. Furthermore, it is concluded that the most appropriate body angle for forward acceleration is $\theta=\pi/4$.

Immediately after this acceleration stage, a possible steady state of the moving body along the horizontal direction is investigated. Primarily, a triangular-wave approximation is considered, where all segments have an orientation $\pm\theta$ relative to the x-direction, and a vertical speed $\pm c\tan\theta$, ensuring a wave phase speed equals to c [*cf.* Fig. 2(a)]. During this stage, the local velocity of the segment within the laboratory frame ceases to be along the vertical, and instead forms the angle α with the body tangent. The steady state is given by the absence of frictional forces along the x-direction, $\boldsymbol{f}\cdot\boldsymbol{e}_x = 0$, *i.e.* $\theta+\beta = \pm\pi/2$, which in Eq. (3), yields

$$\tan(\theta+\alpha) = \frac{1+\frac{\mu_n}{\mu_s}\tan^2\alpha}{2\left(\frac{\mu_n}{\mu_s}-1\right)\tan\alpha} \tag{4}$$

By knowing θ and α, it is possible with geometrical considerations to deduce the velocity expression of the body's center of mass in the laboratory frame: $U/c = \tan\theta/\tan(\theta+\alpha)$. Equation (4) is solved numerically to provide the solution of α and estimate the velocity ratio U/c. Figure 2(b) shows the numerical solution of U/c as a function of θ for different ratios of friction coefficients. It is observed that the normalized speed increases with μ_n/μ_s. Also, U/c increases rapidly with θ, reaching a zone of slow variation located above $\theta\sim50°$, which is maximal for a body orientation of $\theta\sim70-80°$. Thus, this approach predicts the high efficiency of relatively large angles for propulsion.

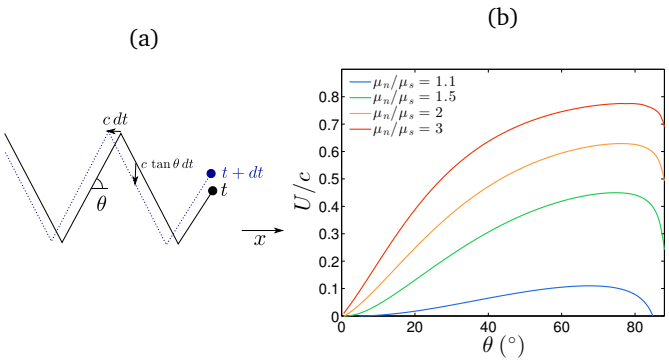

Fig. 2 (a) Sketch of a triangular wave propagating to the left at phase speed c, along a slender body with respect to its own frame. (b) Normalized velocity, U/c, of a body propagating according a triangular wave as a function of the body angle θ and for $\mu_n/\mu_s = 1.1, 1.5, 2, 3$. Solutions are found numerically from Eq. (4) and U/c, obtained through the relation, $U/c = \tan\theta/\tan(\theta+\alpha)$, with $\theta+\beta = 89.5°$.

2.4 Numerical method

The dynamics of a slender body subject to a propagating flexural wave and anisotropic friction forces does not present a simple analytical solution. Thus, it is more appropriate to solve it numerically. The friction force experienced by each segment is projected along the x and y directions, and these projections are integrated along the whole body length, L, providing the total forces F_x and F_y it experiences. Then, the position of the body's center of mass (X,Y) is predicted by integrating the equations of motion, $\rho L\ddot{X} = F_x$ and $\rho L\ddot{Y} = F_y$ through a fourth order Runge-Kutta method. Such relations are due to the fact that the sum of the internal forces $\boldsymbol{f}_{\text{int}}$ exerted by the snake along its body length is null. The mean angular position $\langle\theta\rangle_s = \int_0^L \theta\,ds/L$ of the body over time is determined through torque equilibrium, as detailed by Hu *et al.*[17]. This procedure provides the motion of the body in the laboratory reference frame as a function of the wave angular amplitude θ_m, wave frequency $f=\omega/2\pi$, wavelength $\lambda = 2\pi/k$ and the friction coefficients ratio μ_t/μ_s.

3 Numerical solutions

3.1 Dynamics

The dynamics of the undulating body is solved numerically following the model developed in section 2.4. The motion of the body's center of mass is shown in Fig. 3 as a function of time for a given set of parameters, corresponding to parameters determined by Hu *et al.*[17] for Pueblan milk snakes ($L=0.36$ m, $\rho=0.042$ kg/m, $\theta_m=63°$, $kL/2\pi=1$, $f=0.5$ Hz, $\mu_s=0.11$ and $\mu_n=0.19$). The body's center of mass is observed to move forward along the x-direction and undergoes oscillations, without drift, along the y-direction. Figure 3(b) shows that following the initial few oscillations the body reaches a steady state, where the horizontal velocity, $\dot{X}$, is oscillatory and has a positive mean value. This corroborates the global motion that takes place along the x-direction. Figure 3(a) demonstrates that the horizontal speed predicted in these simulations is more similar to experimental

View Article Online
DOI: 10.1039/C7SM01545C

data from Pueblan milk snakes than Hu's calculations[17]. This fact arises from the factor two in the perpendicular projection of the force as underlined in section 2.2. Finally, the mean locomotion speed U of the body is defined to be in the steady state, as $U = \frac{1}{T}\int_0^T \sqrt{\dot{X}^2+\dot{Y}^2}\,dt$ where $T = 1/f$. For the corresponding set of parameters, examples of local velocities and forces in the steady state over different time periods are shown in Fig. 4. Subsequently, it is ensured that the mean value of the body motion along the x-axis is directly proportional to the wave frequency, consistent with the low inertial regimes common to undulating snakes[17,19]. Moreover, as a check of consistency, the numerical simulation results are verified to be independent from the linear body mass ρ, the time and space resolution.

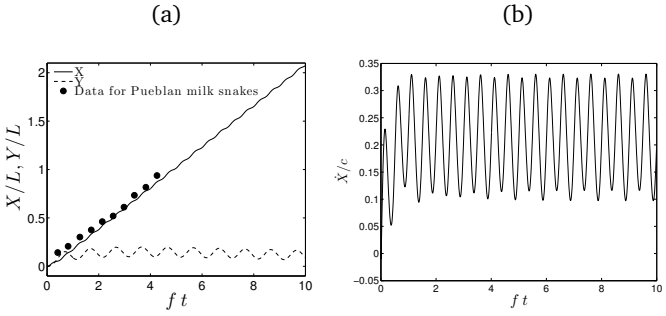

Fig. 3 Numerical simulation to solve the position of the center of mass in an undulating body with $L = 0.36$ m, $\rho = 0.042$ kg/m, $\theta_m = 63°$, $kL/2\pi = 1$, $f = 0.5$ Hz, $\mu_n/\mu_s = 1.72$ ($\mu_s = 0.11$). (a) Normalized horizontal position X/L (solid line) and vertical position Y/L (dashed line) of the body center of mass as a function of the dimensionless time ft. Black dots show the experimental horizontal position of the body center of mass for Pueblan milk snakes extracted from Hu *et al.*[17]. (b) Normalized horizontal velocity $\dot{X}/c$ with $c = \omega/k$ as a function of the dimensionless time.

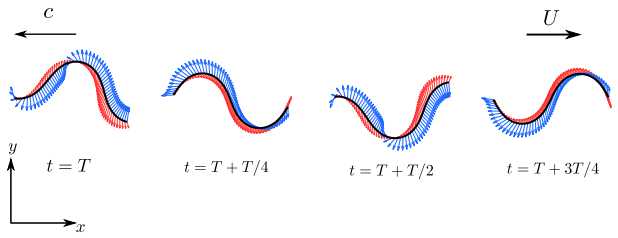

Fig. 4 Numerical simulation of an undulating body in a flexural wave motion, while undergoing anisotropic friction forces. Red arrows indicate local velocity $\boldsymbol{v}$, blue arrows indicte local force per unit length $\boldsymbol{f}$. The parameters of the numerical simulation are: $L = 0.36$ m, $\rho = 0.042$ kg/m, $\theta_m = 63°$, $kL/2\pi = 1.0$, $f = 0.5$ Hz, $\mu_n/\mu_s = 1.72$ ($\mu_s = 0.11$). The wave propagates toward the left and the body propels to the right.

Thereafter, numerical simulations are employed to study the mean velocity U as a function of the problem's parameters. Figure 5 shows the velocity ratio U/c (with $c = \omega/k$ the wave speed) as a function of the friction coefficient ratio μ_t/μ_s. The propulsive speed increases with the friction coefficient ratio, and follows a non-monotonic dependency with the wave angular amplitude θ_m.

The effect of the wave angular amplitude and the wave number is inspected in greater detail in Fig. 6(a) for the same set of

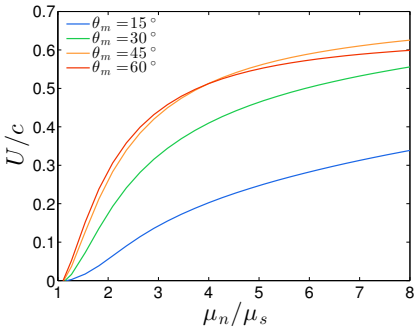

Fig. 5 Normalized mean velocity U/c as a function of the friction coefficient ratio μ_n/μ_s for different wave angles θ_m. The blue, green, orange and red lines correspond respectively to $\theta_m = 15°, 30°, 45°, 60°$. The other parameters are: $L = 0.36$ m, $\rho = 0.042$ kg/m, $kL/2\pi = 1.0$, $f = 0.5$ Hz and $\mu_s = 0.11$.

parameters previously studied. It is clear that the mean velocity U presents local maxima for certain angular amplitudes and wavelengths. These maxima are reached for large angular amplitudes $\theta_m \simeq 65°$ and for wavelengths close to integer numbers of the body length ($\lambda \simeq L, 2L$, etc..). The wave characteristics for an efficient forward speed is comparable to those exhibited by snakes. Thus, the undulating characteristics of Pueblan milk snakes as determined by Hu *et al.*[17] ($\lambda \simeq L$ and $\theta_m \simeq 63°$) are indicated by a white dot in Fig. 6(a). It is noted that the undulating characteristics of Pueblan milk snakes are similar to the first maximum speed predicted by the model.

A further example of propulsion by a traveling wave and anisotropic friction is the motion of sandfish lizards within desert sand. Indeed, Malden *et al.* showed that sandfish lizards are able to propel up to twice their body length per second in sand by undulating their body[31]. Moreover, they proved that the friction force experienced by a cylinder dragged into a granular medium is anisotropic, being larger for a transversal motion than for a longitudinal one. Such experiments reveal that friction anisotropy in a granular material can be approached by two coefficients of friction μ_s and μ_n having a ratio $\mu_n/\mu_s \simeq 2.1$. Also, a similar approach was successfully employed to describe helical locomotion in a granular medium[32]. Figure 6(b) shows the influence of the wave angular amplitude and the wave number on the mean locomotion speed U for such a ratio of friction coefficient. It is apparent that the first optimum of undulating parameters in order to propel forwards ($\theta_m = 54°$ and $\lambda = L$) is similar to the characteristics employed by sandfish lizards ($\theta_m \simeq 51°$ and $\lambda \simeq L$) as reported by Malden *et al.*[31]. It seems that both Publean milk snakes and sandfish lizards use the optimal motion in order to maximize traveling speed for a given frequency of undulation.

Furthermore, the fact larger speeds are reached when the body length is an entire number of wavelengths may be attributed to the stationary distribution of body angle in such a configuration. Indeed, when the body length is not an entire number of wavelengths, the body angle distribution changes with time as the wave propagates, leading to a non-stationary dynamic which reduces the mean moving speed of the body.

View Article Online
DOI: 10.1039/C7SM01545C

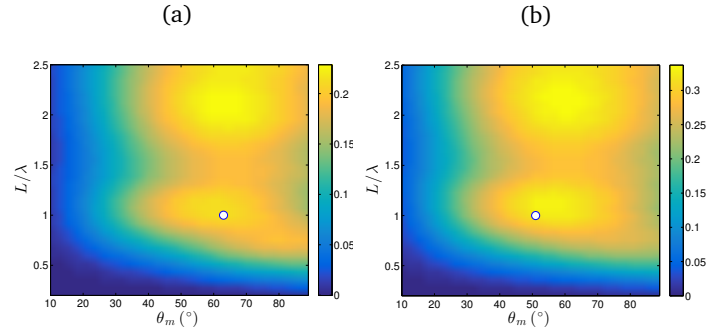

Fig. 6 (a) Normalized mean horizontal velocity U/c as a function of the wave amplitude θ_m and wave number L/λ for $L = 0.36$ m, $\rho = 0.042$ kg/m, $f = 0.5$ Hz, $\mu_n/\mu_s = 1.72$ ($\mu_s = 0.11$). The white dot shows the undulating characteristics used by Pueblan milk snakes as determined by Hu *et al.*[17]. (b) Normalized mean horizontal velocity U/c as a function of the wave amplitude θ_m and wave number L/λ for $L = 0.08$ m, $\rho = 0.20$ kg/m, $f = 2.0$ Hz, $\mu_n/\mu_s = 2.1$. The white dot shows the undulating characteristics used by sandfish lizards as determined by Malden *et al.*[31] ($\theta_m \simeq 51°$ and $\lambda \simeq L$).

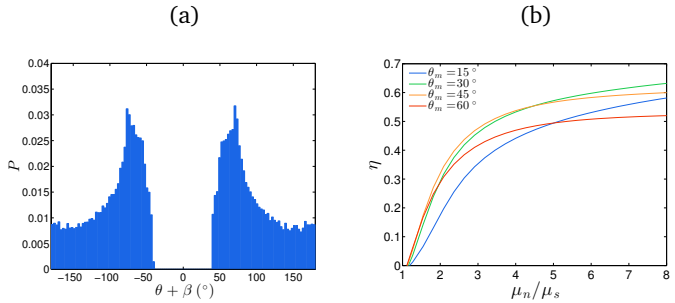

Fig. 7 (a) Probability distribution of the angular orientation $\theta + \beta$ of the friction force relative to the horizontal, for a numerical simulation with $L = 0.36$ m, $\rho = 0.042$ kg/m, $\theta_m = 63°$, $kL/2\pi = 1.0$, $f = 0.5$ Hz and $\mu_n/\mu_s = 1.72$ ($\mu_s = 0.11$). (b) Power efficiency η as a function of the friction coefficient ratio μ_n/μ_s for different wave angles θ_m. The blue, green, orange and red lines correspond respectively to $\theta_m = 15°, 30°, 45°, 60°$. The other parameters are: $L = 0.36$ m, $\rho = 0.042$ kg/m, $kL/2\pi = 1.0$, $f = 0.5$ Hz and $\mu_s = 0.11$.

One remarks that the optimal motion encountered in a flexural wave differs from a triangular one [cf. section 2.3]. This difference may be attributed to the fact that flexural waves contain a large range of body orientations compared to triangular waves, which leads to a more complex steady state. In this steady state, the local orientation of the friction force may differ from the vertical as the constraint of a null horizontal force only applies on the sum of all the forces. The mean distribution of the local force orientation relative to the horizontal, $\theta + \beta$, is obtained numerically and presented in Fig. 7(a) for a specific set of parameters. It is observed that the angular distribution is not centered around $\pm 90°$ and is widely distributed. The difference in propulsion between flexural and triangular waves is due to the difference in the steady states they generate.

For the sake of comparison, we remind briefly some results for undulating locomotion in viscous fluids. According to Berman *et al.*[33], a body of slenderness equals to 1/30, moving in a fluid at low Reynolds numbers, is subjected to forces of anisotropy ratio of about 1.5. The same authors demonstrated that for a sinusoidal body wave, the maximal propulsion speed (at a given frequency) is reached for a wave amplitude of $0.3L$ and a wavelength of $0.7L$.

3.2 Energy consumption

The minimal power required from the body to move is $\mathscr{P} = \int_0^L (\boldsymbol{f}_{\text{int}} \cdot \boldsymbol{v})\, ds$ where $\boldsymbol{f}_{\text{int}} = -\boldsymbol{f}$ under the assumption of negligible inertia. The ratio between the minimal power output $\mu_s \rho L g U$ required by the body to follow its own path and the effective power output is $\eta = \mu_s \rho L g U / f \int_0^T \mathscr{P} dt$. The closer that η is to one, gives a more efficient undulating movement in terms of energy consumption. Figure 7(b) shows η as a function of the friction coefficients ratio μ_n/μ_s. It is apparent that the power efficiency increases with μ_n/μ_s, and follows a non-monotonic dependency to the wave angular amplitude θ_m. Figures 8(a)-(b) present the evolution of η with both the angular amplitude θ_m and wavenumber L/λ for the sets of parameters corresponding to Pueblan milk snakes and sandfish lizards, respectively. The power efficiency η presents local maxima for given sets of angular amplitude and wavelength. These maxima occur for lower angular amplitudes than the ones of the mean body speed [*cf.* Fig. 6]. Regarding the mean horizontal speed, maximum power efficiency is reached when the body length corresponds to an entire number of wavelengths. For figures, larger η values presented in Fig. 8(a) corresponds to an efficiency of about 27%.

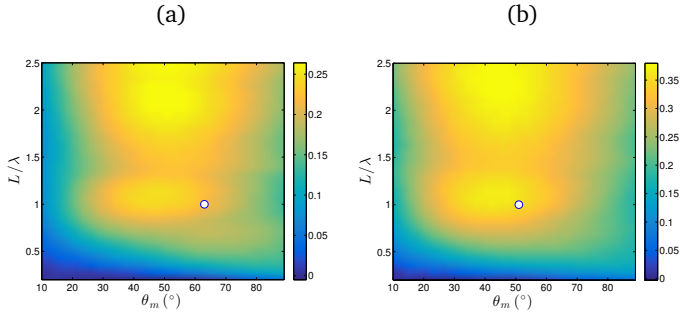

Fig. 8 (a) Power efficiency η as a function of the wave amplitude θ_m and wave number L/λ for $L = 0.36$ m, $\rho = 0.042$ kg/m, $f = 0.5$ Hz and $\mu_n/\mu_s = 1.72$ ($\mu_s = 0.11$). The white dot shows the undulating characteristics of Pueblan milk snakes, established by Hu *et al.*[17]. (b) Power efficiency η as a function of the wave amplitude θ_m and wave number L/λ for $L = 0.08$ m, $\rho = 0.20$ kg/m, $f = 2.0$ Hz, $\mu_n/\mu_s = 2.1$. The white dot shows the undulating characteristics used by sandfish lizards as determined by Malden *et al.*[31] ($\theta_m \simeq 51°$ and $\lambda \simeq L$).

As previously noted, the characteristics of efficient wave motion can be compared to snakes and sand lizards. The white dot in Fig. 8(a) shows the undulating characteristics of Pueblan milk snakes as determined by Hu *et al.*[17] ($\lambda \simeq L$ and $\theta_m \simeq 63°$). Similarly, the white dot in Fig. 8(b) indicates the undulating characteristics of burrowed sandfish lizards ($\theta_m \simeq 51°$ and $\lambda \simeq L$) as determined by Malden *et al.*[31]. One observes that the undulating characteristics of Pueblan milk snakes and sandfish lizards are similar to the prediction of the first maximum in efficiency from the previous model. It is remarkable that while optimizing speed, these animals seen adapted to reach energy consumptions that are very near the optima predicted by the theory. However, the greater distance of snake's undulating parameters to the efficiency optimum

View Article Online
DOI: 10.1039/C7SM01545C

than sandfish's undulating parameters may be attributed to the fact that sandfish lizards are at lower risk from predators when burrowed. Finally, it is noted that legless animals do not use other alternative wavelengths in order to reach greater speeds, probably due to biomechanical constraints as suggested by Guo and Mahadevan[20].

3.3 Following its own path

A specific case has been addressed by Guo and Mahadevan, where an undulating body follows its own path while including internal visco-elastic constraints[20]. The same problem is considered here for a slender body moving with a travelling flexural wave and subjected to anisotropic friction. In such a situation, the friction coefficient ratio μ_n/μ_s is sufficiently large to minimize lateral sliding. As a consequence, the friction force writes $\boldsymbol{f} = -\rho g \mu_s \boldsymbol{e}_s - f_n \boldsymbol{e}_n$ where the transversal force f_n remains undetermined. Thus, we use the fact that the sum of internal body forces is null which leads to $\int_0^L \boldsymbol{f} ds = \boldsymbol{0}$ and assume a non-inertial regime. Projecting the previous relation in the $x-y$ base, the following is derived: $\int_0^L f_n \sin\theta \, ds = \rho g \mu_s L_x$ where $L_x = \int_0^L \cos\theta \, ds$. The simplest solution respecting the conditions of this equation is, $f_n = \gamma \sin\theta$, that can be introduced into the previous relation and gives to the following expression of the peak force:

$$f_{n,m} = \rho g \mu_s k L_x \frac{\sin\theta_m}{\int_0^{2\pi} \sin^2\left[\theta_m \sin(s')\right] ds'}. \qquad (5)$$

The numerical solution of Eq. (5) is presented as a function of the angular amplitude θ_m in Fig. 9(a). It is apparent that a greater angular amplitude θ_m, allows for a reduced normal peak force $f_{n,m}$ to follow the wave motion. Assuming that $\theta_m \ll 1$, Eq. (5) is developed at the first order and yields $f_{n,m} \simeq \rho g \mu_s k L_x / \pi \theta_m$. Such an approximation is plotted in Fig. 9(a) and is observed to give an accurate description of the solution. Above $\theta_m \simeq 30°$, the normal peak force decreases gradually along with the angular amplitude. This implies that angular amplitudes larger than $\theta_m \simeq 30°$ are not so advantageous to animals and robots which operate under the context of reducing normal forces. Besides, for Pueblan milk snakes the transversal sliding criteria ($f_{n,m} = \rho g \mu_n$) is indicated by the way of the dashed black line in Fig. 9(a). One observes that the normal peak force $f_{n,m}$ is larger than the sliding criteria up to $\theta_m = 75°$. In practice, lateral sliding is prevented by slithering snakes over sand substrates as it can lead to the accumulation of material in the transversal direction, thus generating additional normal resistance[12].

3.4 Body lift

Previous studies have reported that snakes lift the curved parts of their body during slithering[6,17]. This phenomenon has been considered by Hu *et al.*[17] by including a non-uniform linear mass within simulations. It was shown that through modulating the mass distribution, snakes can increase their forwards speed by up to 50%. In order to account for this lifting capacity, a threshold in curvature was introduced into the previous numerical simulation, κ_s, above which no friction forces apply (the body curvature being defined as $\kappa = \partial\theta/\partial s$). Furthermore, the weight of lifted

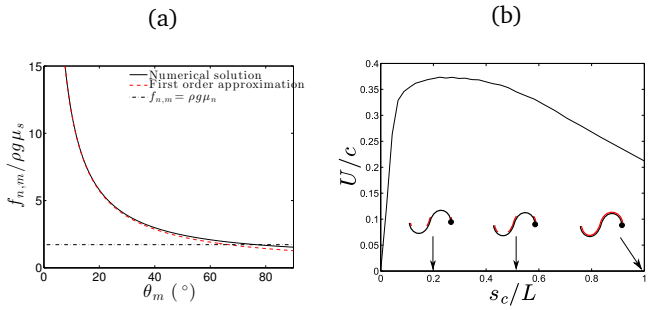

Fig. 9 (a) Normalized peak normal force $f_{n,m}/\rho g \mu_s$ as a function of the angular amplitude θ_m for an undulating body that does not slide laterally. The black solid line shows the numerical solution of Eq. (5) and the red dashed line denotes the first order approximation. The black dotted line indicates the normal peak force reaching the sliding criteria ($f_{n,m} = \rho g \mu_s$). (b) Normalized mean speed of the undulating body U/c as a function of the fraction of the body length in contact with the ground s_c/L. Simulations are run according to the model developed in section 2, however the force is considered null for segments presenting a curvature exceeding the curvature threshold κ_t. The parameters of the numerical simulation are: $L = 0.36$ m, $\rho = 0.042$ kg/m, $\theta_m = 63°$, $kL/2\pi = 1.0$, $f = 0.5$ Hz, $\mu_n/\mu_s = 1.72$ ($\mu_s = 0.11$). The three sketches in red indicate the body segments in contact with the ground for the corresponding curvature threshold.

segments was redistributed uniformly along the segments in contact with the ground. Figure 9(b) shows the calculated mean horizontal speed of the body as a function of the fraction of the body length in contact with the ground, s_c/L. A body permanently in contact with the substrate ($s_c/L = 1$) is provided by $\kappa_t = \max_s(\kappa)$. One observes in Fig. 9(b) that a reduction in the length of body in contact with the ground increases the mean horizontal speed of the body. Such an effect persists for up to a contact length of about 40% of the body length in contact with substrate. For lower contact fractions, the mean speed reaches a plateau prior to decreasing, due to the absence of propulsive force. This result demonstrates that snake propulsion is provided by segments having a low curvature, and explains why snakes lift the curved parts of their body to slither faster and more efficiently.

3.5 Slope climbing

This section considers the case where the substrate presents a slope of angle ϕ relative to the horizontal. Through modification of the force balance presented in section 3.1 (the force experienced by each segment writes in the plane of motion $\boldsymbol{f} = -\rho\, g \cos\phi \left[\mu(\alpha)\boldsymbol{e}_v + \mu'(\alpha)\boldsymbol{e}_{v_\perp}\right] - \rho\, g \sin\phi\, \boldsymbol{e}_x$), it was possible to obtain the effect of the slope on the overall motion of the undulating body. The results of this study are presented in Fig. 10, where the normalized mean velocity U/c of the body along the slope is plotted as a function of ϕ, for a given set of parameters corresponding to Pueblan milk snakes, and for two different contact situations. In the case where the entire body is permanently in contact with the ground ($s_c/L = 1$), it is noted that the mean velocity of the body decreases with ϕ up to zero for $\phi_c = 2.5°$. Above the critical angle ϕ_c, the body cannot climb uphill and slides downwards. The same procedure has been carried out in the case where the segments of the body with a curva-

View Article Online
DOI: 10.1039/C7SM01545C

ture exceeding 50% do not experience friction (corresponding to a contact fraction of $s_c/L = 0.33$). In such a situation, the maximal accessible slope increases to $\phi_c = 4.0°$. In addition to an increase in velocity, lifting curved sections also supports slithering snakes to climb steeper slopes. The maximal slope ϕ_c can be approached theoretically by equalizing the maximal propulsive force $2\rho g(\mu_n - \mu_s)\cos\theta\sin\theta$ with the horizontal component of the weight $\rho g \sin\phi$. This consideration yields $\sin\phi_c = \mu_n - \mu_s$, which results in $\phi_c = 4.6°$ for Publean milk snakes. Therefore, it is shown that snakes which effectively lift a part of their body are able to climb a slope close to this theoretical limit. However, the maximal slope a snake can climb using a slithering motion is relatively small compared to the slopes encountered in natural environments. For example in sandy deserts, the typical avalanche angle of dunes ranges from 30° to 40°[34]. In order to progress through a sloped environment, snakes adopt another mode of locomotion known as sidewinding[12]. The main difference between the sidewinding and the slithering is that sidewinding does not involve a sliding motion, and instead involves static friction with the ground. Consequently, the maximal slope that a snake is able to climb using sidewinding is given by the equilibrium of static forces as by $\tan\phi_c = \mu_n$. For $\mu_n = 0.19$, it yields $\phi_c = 10.8°$. Furthermore, in the case of sandy slopes, the substrate deformability induces an extra resistance to sliding and increases ϕ_c, reaching about 20° for sidewinder rattlesnakes[12].

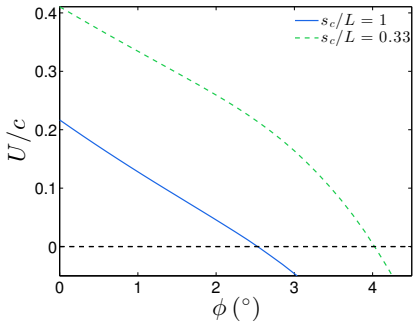

Fig. 10 Normalized mean speed of an undulating body U/c as a function of the slope inclination ϕ. The parameters of the numerical simulations are: $L = 0.36$ m, $\rho = 0.042$ kg/m, $\theta_m = 63°$, $kL/2\pi = 1.0$, $f = 0.5$ Hz and $\mu_n/\mu_s = 1.72$ ($\mu_s = 0.11$). The blue solid line represents a situation where the entire body is in contact with the substrate ($s_c/L = 1$) and the green dashed line represents the case with a third of the body length in contact with the ground ($s_c/L = 0.33$).

Conclusion

This study focused on the propulsive motion of a slender body subjected to a lateral traveling wave and anisotropic friction forces. The optimal wave characteristics to which maximize the mean forwards speed and minimize the total energy consumption was observed. In the animal kingdom, Pueblan milk snakes and Sandfish lizards adopt undulating characteristics to maximize speed. In addition, these numerical simulations highlighted the body parts which contribute efficiently to propulsion, and explain why snakes lift their curved segments while slithering. Finally, slithering locomotion has been proved to be ineffective for climbing slopes steeper than few degrees, which leads to the explanation for the use of the sidewinding gait in such a context.

More generally, a better understanding of the different gaits employed by snakes will help to development of snake robots, which may prove as useful tools in rescue missions within confined spaces[27], and for exploration of complex environments such as planets and asteroids. However, several aspects of snake locomotion remain poorly understood and require further studies. For example, the context under which slithering is preferred to sidewinding by snakes remains to be investigated. Also, the physical origin of the friction anisotropy is still an open problem and requires further investigation. This last point is crucial for the development of artificial textures with a high friction anisotropy that could be used to mimic the slithering mode of locomotion with robots. In conclusion, contrary to leg or wheel locomotion, legless gaits remains poorly understood and facing this challenge may lead to the development of novel strategies to succeed complex locomotion tasks.

Acknowledgments

B.D.T. acknowledges the support of the CONICYT-Chile postdoctoral fellow Fondecyt: 3160167. F. M. is grateful to Proyecto Basal: 1555 of Universidad de Santiago. The authors sincerely thank Tania Sauma for careful reading and helpful comments.

References

1 J. Gray, *Animal locomotion*, Weidenfeld & Nicolson, 1968.
2 A. A. Biewener, *Science*, 1990, **250**, 1097.
3 M. H. Dickinson, C. T. Farley, R. J. Full, M. A. R. Koehl, R. Kram and S. Lehman, *Science*, 2000, **288**, 100–106.
4 R. Alexander, *Principles of animal locomotion*, Princeton University Press, 2003.
5 G. K. Taylor, R. L. Nudds and A. L. R. Thomas, *Nature*, 2003, **425**, 707–711.
6 C. Gans, *Herpetologica*, 1986, **42**, 33–46.
7 B. Chan, N. J. Balmforth and A. E. Hosoi, *Physics of Fluids (1994-present)*, 2005, **17**, 113101.
8 K. J. Quillin, *Journal of Experimental Biology*, 1999, **202**, 661–674.
9 B. C. Jayne, *Copeia*, 1986, 915–927.
10 H. Marvi and D. L. Hu, *Journal of The Royal Society Interface*, 2012, **9**, 3067–3080.
11 S. M. Secor, B. C. Jayne and A. F. Bennett, *Journal of experimental biology*, 1992, **163**, 1–14.
12 H. Marvi, C. Gong, N. Gravish, H. Astley, M. Travers, R. L. Hatton, J. R. Mendelson, H. Choset, D. L. Hu and D. I. Goldman, *Science*, 2014, **346**, 224–229.
13 H. W. Lissmann, *Journal of Experimental Biology*, 1950, **26**, 368–379.
14 M. Walton, B. C. Jayne and A. F. Bennett, *Science*, 1990, **249**, 524–527.
15 H. Marvi, J. Bridges and D. L. Hu, *Journal of The Royal Society Interface*, 2013, **10**, 20130188.
16 J.-P. Gasc and C. Gans, *Copeia*, 1990, 1055–1067.

View Article Online
DOI: 10.1039/C7SM01545C

17 D. L. Hu, J. Nirody, T. Scott and M. J. Shelley, *Proceedings of the National Academy of Sciences*, 2009, **106**, 10081–10085.
18 F. Jing and S. Alben, *Physical Review E*, 2013, **87**, 022711.
19 S. Alben, Proc. R. Soc. A, 2013, p. 20130236.
20 Z. V. Guo and L. Mahadevan, *Proceedings of the National Academy of Sciences*, 2008, **105**, 3179–3184.
21 E. Lauga and T. R. Powers, *Reports on Progress in Physics*, 2009, **72**, 096601.
22 J. Elgeti, R. G. Winkler and G. Gompper, *Reports on progress in physics*, 2015, **78**, 056601.
23 J. Gray and G. J. Hancock, *Journal of Experimental Biology*, 1955, **32**, 802–814.
24 U. B. Kaupp and L. Alvarez, *The European Physical Journal Special Topics*, 2016, **225**, 2119–2139.
25 R. E. Johnson and C. J. Brokaw, *Biophysical journal*, 1979, **25**, 113–127.
26 B. Rodenborn, C.-H. Chen, H. L. Swinney, B. Liu and H. P. Zhang, *Proceedings of the National Academy of Sciences*, 2013, **110**, E338–E347.
27 G. S. P. Miller, *Neurotechnology for Biomimetic Robots*, 2002, 271.
28 D. Chateau and J.-C. Géminard, *Physical Review E*, 2013, **88**, 033202.
29 F. Tapia, D. Le Tourneau and J.-C. Géminard, *EPJ Techniques and Instrumentation*, 2016, **3**, 1.
30 D. L. Hu and M. Shelley, *Natural locomotion in fluids and on surfaces*, Springer, 2012, pp. 117–135.
31 R. D. Maladen, Y. Ding, C. Li and D. I. Goldman, *Science*, 2009, **325**, 314–318.
32 B. Darbois Texier, A. Ibarra and F. Melo, *Physical Review Letters*, 2017, **119**, 068003.
33 R. S. Berman, O. Kenneth, J. Sznitman and A. M. Leshansky, *New Journal of Physics*, 2013, **15**, 075022.
34 M. A. Carrigy, *Sedimentology*, 1970, **14**, 147–158.

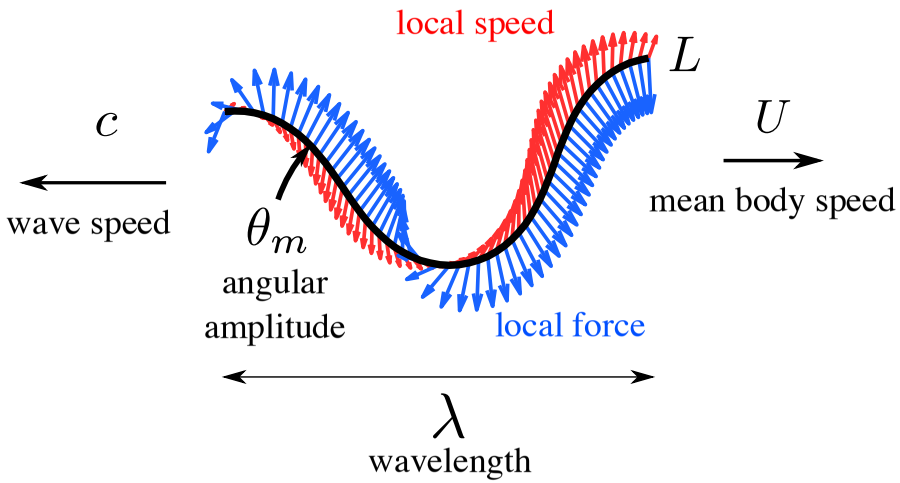

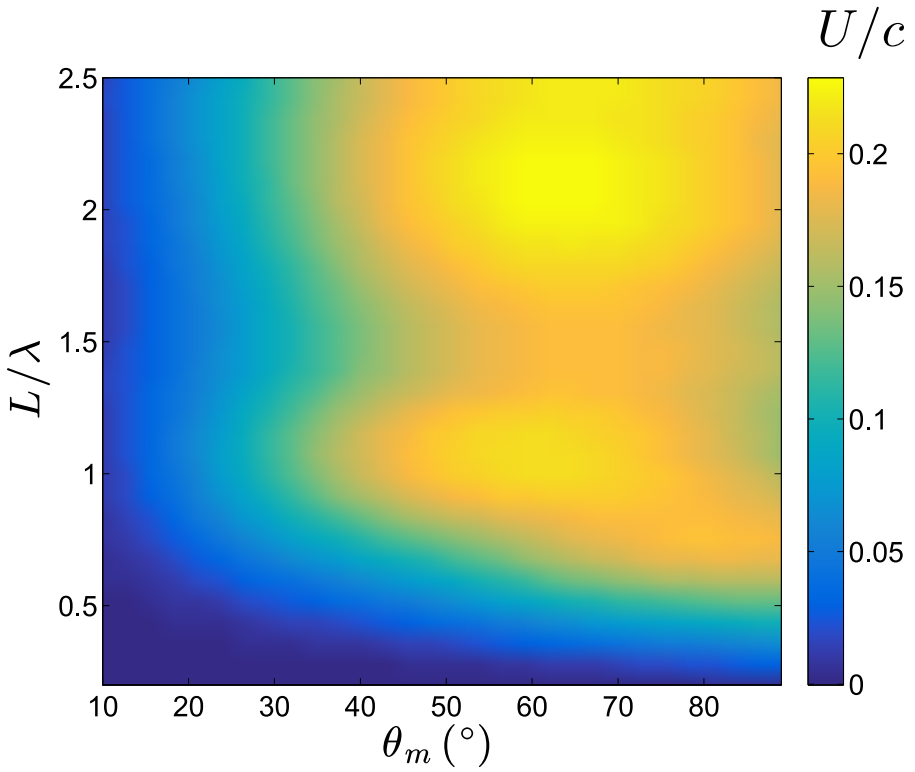

We found numerically the optimal undulating motion for a slender body to propel through anisotropic friction forces.